Shear Dispersion in Combined Pressure-Driven and Electro-Osmotic Flows in a Capillary Tube with a Porous Wall

Morteza Dejam, Hassan Hassanzadeh, and Zhangxin Chen
Dept. of Chemical and Petroleum Engineering, Schulich School of Engineering, University of Calgary, 2500 University Drive NW, Calgary, AB, Canada T2N 1N4

DOI 10.1002/aic.14897
Published online June 16, 2015 in Wiley Online Library (wileyonlinelibrary.com)

An analytical expression is derived for the shear dispersion during transport of a neutral nonreacting solute within a coupled system comprised of a capillary tube and a porous medium under the combined effects of pressure-driven and electro-osmotic flows. We use the Reynolds decomposition technique to obtain a dispersion coefficient by considering a sufficiently low wall or zeta potential that accounts for the combined flows. The coupled dispersion coefficient depends on the Debye–Hückel parameter, Poiseuille contribution fraction, and Péclet number. The developed model also provides a shear dispersion coefficient for an impervious capillary tube (noncoupled system). The ratio of the coupled (porous wall) and noncoupled (impervious) dispersion coefficients reveals that it is essential to include the transport of chemical species from the tube to the porous medium in several important physical situations. These findings have implications for design of chemical species transport in porous microfluidic networks and separation of emulsions in microchannel-membrane systems. © 2015 American Institute of Chemical Engineers *AIChE J*, 61: 3981–3995, 2015
Keywords: capillary tube, porous wall, coupled system, pressure-driven, electro-osmotic, combined flow, shear dispersion

Introduction

The two processes of mixing and separation act against each other in many operating circumstances in an elution process. Mechanisms like diffusion and dispersion prevent separation whereas they help mixing. Improving the performance of either mixing or separation has motivated numerous theoretical and experimental studies to investigate dispersion in electro-osmotic flow (EOF) with[1–4] or without[5–16] existence of pressure-driven flow. The EOF, which is generally preferred over pressure-driven flow in separation processes, is generated by an electric field accompanied with the electric double layer (EDL) formed close to a wall due to the ionic nature of an electrolyte carrying a chemical species. The thin EDL is valid for most aqueous systems because the Debye length (a measure of the EDL thickness) is only a few nanometers (1–10 nm) in such cases.

As compared with transport in pressure-driven flow, the most important advantages of EOF under the condition of a thin EDL is associated with producing a much weaker dispersion of a solute matter leading to more efficient separation. The Taylor[17] dispersion happens due to the shear flow (or velocity variation in the transverse direction) within a capillary tube. The EOF produces relatively weak dispersion as the electro-osmotic velocity profile is almost plug-like (flat) within the capillary tube except within the thin EDL. Taylor and Yeung,[18] Herr et al.,[19] and Tallarek et al.[20] experimentally verified the plug-like velocity profile of the EOF. In contrast, the pressure-driven flow resembles a parabolic velocity profile and, consequently, generates much stronger dispersion in the case of a high velocity (or Péclet number). This significant difference between pressure-driven and EOF flows results in the latter as a potential technique for separation, in which dispersion is undesirable. However, it is not easy to create a purely EOF while dealing with microfluidic networks[1–16,21] and, therefore, the EOF is generally accompanied with the pressure-driven flow due to several mechanisms.[22] Although the pressure-driven flow is expected to be much weaker than the EOF (main flow) in the applications of interest, nevertheless, it contributes considerably to the dispersion of a chemical species as a result of the parabolic shape of the velocity profile. In the case of purely pressure-driven flow, the effects of several conditions at the tube wall (e.g., no-flux,[17,23,24] adsorbing,[23,25] permeable,[26–28] and porous[28–32]) were investigated while in the case of the purely electro-osmotic and combined electro-osmotic and pressure-driven flows, the studies of the effects of the no-flux,[1–3,5–15] adsorbing,[4,16,33,34] porous,[21,35,36] and permeable[21,35,36] conditions at the tube wall are still very limited.

Datta and Kotamarthi[1] derived a dispersion coefficient for a capillary tube with a nonporous wall that accounts for the combined effects of pressure-driven and EOFs. They introduced a new parameter as the fraction of the combined flows contributed by pressure-driven flow, which made the analysis easier.[1] Assuming a sufficiently low wall or zeta potential, Datta,[5] McEldoon and Datta,[6] and Griffiths and Nilson[7] evaluated a dispersion coefficient for EOF within the tube and parallel plates with a no-flux boundary condition at the wall.[5–7]

Correspondence concerning this article should be addressed to H. Hassanzadeh at hhassanz@ucalgary.ca.

© 2015 American Institute of Chemical Engineers

Zholkovskij et al.[9] interpreted the dispersion of a nonelectrolyte solute due to the EOF in a long straight microchannel using a thin EDL for arbitrary wall or zeta potential.[9] Hydrodynamic dispersion due to the electro-osmotic and combined flows through microchannels under the condition of a thin EDL for an arbitrary wall or zeta potential, electrolyte type, and geometry of a cross-section was addressed by Zholkovskij and Masliyah.[3]

Dutta and Leighton[2] investigated the effect of channel sidewalls on longitudinal dispersion in combined flows. Their results revealed that the flow, wall retention, and the interaction between the two clearly contribute to the slug dispersion in the mobile phase for any arbitrary channel geometry.[2] Later, Huang and Lai[11] theoretically studied mass transport driven by EOF in a two-dimensional (2-D) microchannel and discussed their results based on the velocity and concentration profiles in the channel.[11] Thereafter, Datta and Ghosal[4] studied three sources of dispersion, including inhomogeneous flow fields, solute wall interactions, and force fields normal to channel walls in details. They also discussed microfluidic and nanofluidic applications of their work to capillary electrophoresis, chromatography, and field-flow fractionation.[4] Subsequently, Ramon et al.[12] theoretically studied mass transfer in an EOF for the case of a cylindrical tube with a reactive wall. They derived an analytical expression for the dispersion coefficient, reflecting the time-averaged mass flux of an electrically neutral solute.[12]

Paul and Ng[13] reported an analytical study for the dispersion of a neutral solute released in a 2-D channel with an EOF arising from an electric field interacting with two walls.[13] Later, Paul and Ng[14] performed an analytical study on the time development of hydrodynamic dispersion of an inert species in EOF through a rectangular channel. The objective of their work was an investigation of the effect of the channel side walls on the dispersion coefficient.[14] Subsequently, Ng and Zhou[15] performed an analysis for the dispersion of a neutral nonreacting solute due to EOF through a circular channel under the combined effects of longitudinal nonuniformity of a wall or zeta potential and hydrodynamic slippage on the channel wall.[15]

Ghosal[33] presented a theoretical model for the EOF of solute species when the wall or zeta potential is locally modified by adsorption of the species onto the wall from the carrying electrolyte.[33] Later, Datta and Ghosal[34] generalized the asymptotic theory developed by Ghosal[33] to take into account a slow axial variation in a cross section and arbitrary cross-sectional shapes.[34] Recently, Song et al.[16] theoretically investigated dispersion in EOF in a microchannel under the effect of kinetic sorptive exchange at walls (made up of different materials) using the homogenization method. They analytically derived a general expression for the Taylor dispersion coefficient under different zeta potentials as well as various sorption conditions at the walls.[16] In this work, a combined pressure-driven and EOF within a capillary tube with a porous wall is considered.

Transport in microfluidic networks and several other applications[4,16,33–44] may involve interaction of more than one medium. For example, a capillary tube may be surrounded with a porous medium, which interacts with the fluid inside the capillary tube. However, to the best of our knowledge the influence of the porous tube wall on a dispersion coefficient during solute transport under the combined effects of pressure-driven and EOFs was not studied until now. The previous analytical studies on determination of the dispersion coefficient in a coupled system, resembling a capillary tube with a porous wall, have been traditionally based on the assumption of no interaction between the capillary tube and porous medium. This so-called noncoupled approach resembles a capillary tube with an impervious wall with a no-flux boundary condition at the wall.

This work aims to improve the previous theoretical studies by taking into account the interaction between a porous medium and a capillary tube in determination of a shear dispersion coefficient due to the combined pressure-driven and EOFs. To achieve this, we start with a 2D coupled system, in which the interaction between the capillary tube and porous medium is handled by imposing the continuity of concentration and mass flux at the porous wall. Then, the Reynolds decomposition method is applied to develop an equivalent one-dimensional (1-D) model for advective-dispersive transport with equivalent transport coefficients such as the dispersion coefficient and the equivalent advection term. This work provides a more representative shear dispersion coefficient, which can be used in modeling of solute transport in a capillary tube surrounded by porous media.

Transport of solute through a capillary tube with a porous wall can result in less dispersion compared with that of a nonporous wall of the same dimensions.[28,32] Moreover, due to mass exchange between the capillary tube and porous medium the effective velocity in a capillary tube with a porous wall is greater than that of a nonporous wall.[28,32] Thus, determinations of transport coefficients (including correct dispersion coefficient and effective velocity), which considerably affect on the solute transport, are crucial. Because of these characteristics, study of dispersion in a capillary tube with a porous wall under the combined effects of pressure-driven and EOFs can be of great importance for many applications. In the following, some of these applications are discussed.

The dispersion in a capillary tube with a porous wall in microfluidic networks offers significant practical applications. Various applications of the combined pressure-driven and electro-osmotic or purely electro-osmotic effects to control fluid flow, chemical species transport, and associated processes in porous microfluidics devices, porous microtubes, and parallel porous plates are reported in literature.[21,35,36]

Scales and Tait[21] presented analytical solutions for combined pressure-driven and EOFs in the form of a channel with porous walls using the linearized Poisson–Boltzmann equation with application to porous microfluidics devices.[21] Subsequently, Vennela et al.[36] studied mass transfer of a neutral solute due to combined pressure-driven and EOFs in a microchannel with porous walls. They used a 2-D steady state advection-diffusion equation in a microchannel, in which advection is considered in longitudinal and transversal directions while diffusion is included in transversal direction. Vennela et al.[36] imposed the role of porous walls through the Robin boundary condition at the interface between the microchannel and porous medium.[36] Later, Vennela et al.[35] extended their work to study mass transfer of a neutral solute due to pressure-driven and EOFs in a microtube with a porous wall.[35] The main purpose of these two works was to obtain analytical expressions for Sherwood number in these coupled systems.[35,36]

A relevant application of chemical species transport under EOF through a porous microchannel is electrically assisted transdermal drug delivery, which is one of the newest

promising drug delivery systems.[45–55] This process includes controlled and facilitated transport of drugs (e.g., insulin, nitroglycerin, or testosterone) into the skin or tissue under the effect of an electrical potential gradient.

This work finds applications such as those described by Scales and Tait[21] and Vennela et al.[35,36] for fluid flow through porous microfluidics networks and mass transfer in microchannels and microtubes with porous walls. Another application of the present analysis is separation of microemulsions in a membrane where a dilute emulsion can be subjected to an external electric field in a microchannel with porous walls.[56,57] During the separation, some of the suspended droplets are attracted to the porous walls and pass through the membrane. This process offers practical applications addressing separation of the components of a microemulsion.[56,57]

Revil and Pessel[37] addressed the validity of the classical transport equations in shale containing porous media where the combined pressure-driven and EOF exist using an EDL for low wall or zeta potential (<50 mV). Their investigation has many important applications such as measurements and evaluations of self-potential, electrical logging of hydrocarbon wells, disposal sites of waste materials, removal of contaminates from shales, accurate measurements of permeability of tight and shale formations, dewatering of shaly soils. In all these applications, an EOF is created due to the flow of pore water through shale containing porous media under an electrical field or an electrical current density. With current interest in extraction of hydrocarbons from tight and shale formations, application of electro-osmotic transport for determination of permeability of tight and shale rocks and electrical well logging of these formations becomes necessary and poses very significant and challenging research topics.

This study has the following main features. First, an analytical expression is developed for the shear dispersion during transport of a neutral nonreacting solute within a coupled system comprised of a capillary tube and a porous medium under the combined effects of pressure-driven and EOFs by considering a sufficiently low wall or zeta potential. Second, it provides a model for determination of delivery of a chemical species to porous media surrounding a capillary tube.

The outline of the article is as follows: First, the theoretical model and solutions are presented. Then the results are discussed, followed by a summary and conclusions.

Theoretical Modeling

In this section, after description of the studied physical system, the governing equations of fluid flow and solute transport are described. Then, the Reynolds decomposition method is used to reduce the 2-D solute transport model and obtain an equivalent 1-D model for advective-dispersive transport in the capillary tube. Finally, the analytical expressions for the dispersion coefficients in noncoupled and coupled systems are presented and discussed.

Assumptions and description of the physical model

Consider a horizontal capillary tube of radius R and length L surrounded by a porous medium of thickness ΔR shown in Figure 1. A 2-D cylindrical coordinate system (x, r) is adopted with the origins of the axial and radial directions at the inlet and center of the capillary tube, respectively. The capillary tube is connected between two reservoirs of an electrolyte (or buffer) with an induced or applied electric field (E) across it. A concentration C^* of the solute is introduced instantaneously at time zero (as a pulse) at the inlet of the capillary tube ($x = 0$). Under these circumstances, two processes, including electrophoresis and electro-osmosis, may be created. The electrophoresis is the movement of ions (cations and anions) under the influence of an electric field, which results in the electrophoretic velocity (different for each species of the solute). As cations have positive and anions have negative charges, these species move in opposite directions. Cations move toward the cathode (−) where the detector is typically located. Cations of larger charge and of smaller size move at a faster rate than larger cations with smaller charges. Anions move toward the anode (+) and neutral species do not experience the electrical field. The electro-osmosis is the electrically driven motion of all species relative to the wall of the capillary tube, which leads to the bulk electro-osmotic velocity, u_e (the same for all solute species except in the EDL region). In the case of the very small electrolyte concentration, the presence of the electrolyte does not alter the local conductivity. In other words, the solute is neutral and nonretained (or nonreacting) that does not have strong coulombic forces or adsorptive interaction with the wall of capillary tube as the electro-osmotic velocity is considerably greater than the electrophoretic velocity of most species.[1,15,58] Therefore, under these conditions the electrophoretic velocity can be assumed negligible compared with the electro-osmotic velocity. In addition, a pressure gradient ($dp/dx = \Delta p/L$) exists along the capillary tube, which gives rise to a bulk pressure-driven flow with velocity of u_p. The pressures at the inlet and outlet of the capillary tube are assigned by p_{in} and p_{out}, respectively. As a result, the combined velocity becomes $u = u_p + u_{\text{e}}$, which demonstrates that the solute species move at various velocities under the effects of the electric field and pressure gradient, leading to separation, and are eluted and detected at the outlet of the capillary tube ($x = L$). However, transport of a chemical species from the fluids inside the capillary tube to the surrounding porous medium may happen and affect the dispersion, which is the theme of this study.

The important assumptions involved in this study are as follows:

1. The transport of chemical species from the fluids inside the capillary tube to the porous medium is handled by the continuity of concentrations and mass fluxes at the interface.
2. The system is isothermal.
3. The Reynolds number is much smaller than unity, which means that the inertial term is negligible compared with the viscous term and the flow is laminar.[59]
4. By assuming that the tube length is much larger than the tube radius, the axial velocity has to be significantly larger than the radial velocity; and therefore, the fluid flow is nearly 1-D. This assumption is necessary for determination of dispersion coefficient using the Taylor approach.[60,61]
5. The electrolyte is symmetric binary, which consists of two types of ions of equal and opposite charge (e.g., Na^+Cl^-).
6. The electrolyte concentration is very low and the presence of the electrolyte does not alter the local conductivity. In other words, the solute is neutral and non-nonreacting and there is no solute adsorption on the wall of the capillary tube.
7. The physical properties of the electrolyte solution remain constant throughout the system.
8. The electric field and pressure gradient are uniform in the capillary tube surrounded by the porous medium.

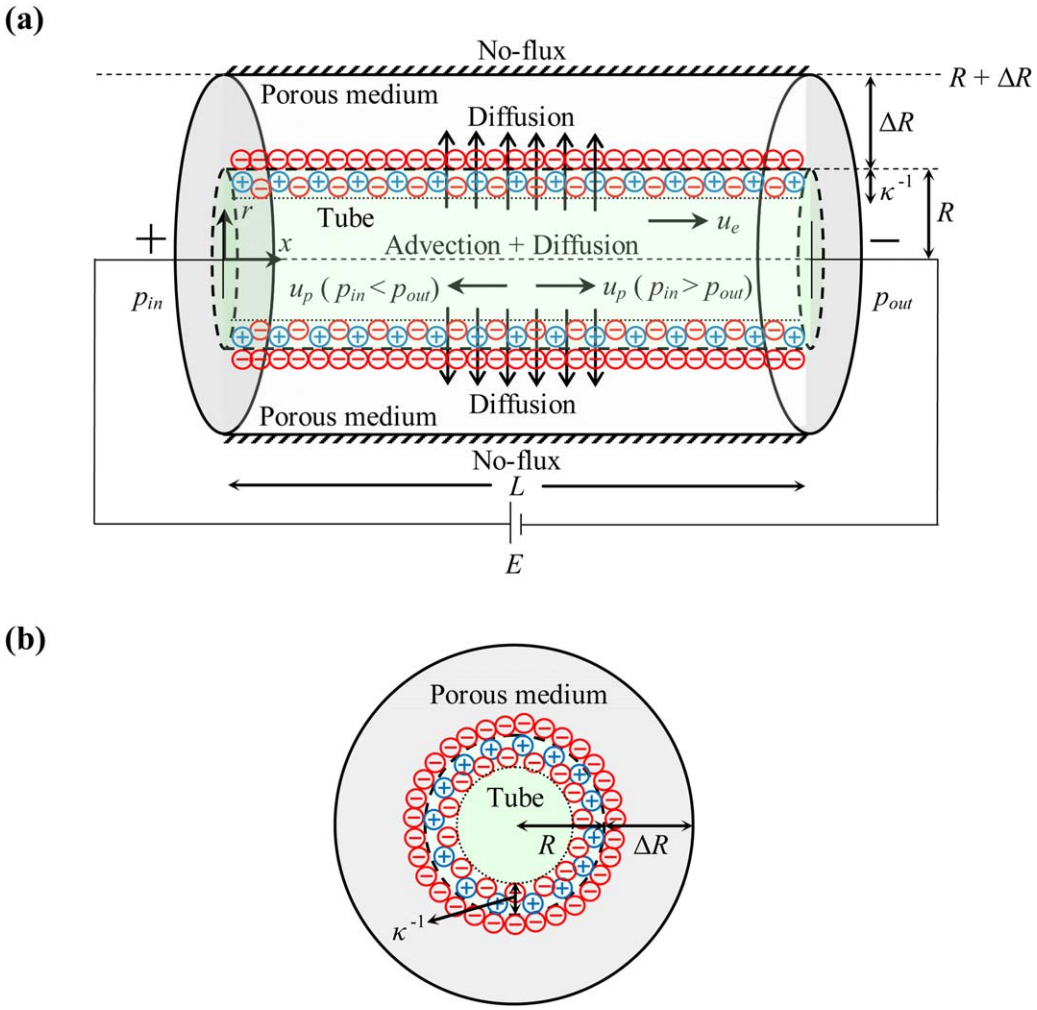

Figure 1. (a) Configuration of the physical model for a coupled system comprised of a capillary tube and a porous medium and (b) cross-section view of the physical model.

[Color figure can be viewed in the online issue, which is available at wileyonlinelibrary.com.]

9. The electric potential in the EDL of thickness κ^{-1} follows the Poisson equation.

10. The charge density in the EDL of thickness κ^{-1} follows the Boltzmann distribution.

11. For sufficiently low wall or zeta potential ($<<25$ mV), the Debye–Hückel linearization holds valid.[61]

12. The wall or zeta potential is assumed to be constant during the mass transfer between the capillary tube and porous medium.

Some of the assumptions aforementioned (8–12) have been adopted to make the problem analytically tractable. More importantly, application of these assumptions for the EDL in the vicinity of a porous wall needs further investigations. There may be a difference between the nature of the EDL for the porous and nonporous walls. In the case of the porous wall, a small discontinuity exists at the interface between the capillary tube and porous medium. The solution of the standard Poisson–Boltzmann equation along with the Debye–Hückel approximation (or linearization) may not be applicable here as this approach is technically applicable for the EDL at an infinite flat plate. However, for model presented in this work, it is assumed that the EDL formed near the wall of capillary tube is thin enough that it does not extend beyond the interface between the two media. This assumption has been extensively used for noncoupled (conduit with nonporous walls)[1–3,5–15] and coupled (conduit with porous walls)[21,35,36] systems. The used assumption in this study was recently applied by Vennela et al.[35,36] to obtain analytical expressions for Sherwood number in coupled systems, including microchannel[36] and microtube[35] with porous walls. However, to the best of our knowledge there is no explicit analytical expression available in the literature that takes into account the porous nature of the wall for EDL.

Governing equations

In this subsection, the governing equations that cover fluid flow and chemical species transport through a capillary tube with a porous wall are described.

Fluid Flow. The dimensionless combined velocity, u_D, in the capillary tube can be presented in terms of the dimensionless pressure-driven velocity, u_{pD}, and electro-osmotic velocity, u_{eD}, as follows[1]

$$u_D(r_D)=u_{pD}(r_D)+u_{eD}(r_D)=2\omega\,(1-r_D^2)+f_e(1-\omega)\left[1-\frac{I_0(\kappa_D r_D)}{I_0(\kappa_D)}\right] \tag{1}$$

where $f_e = 1/(1-2\lambda)$, $\lambda = (1/\kappa_D)I_1(\kappa_D)/I_0(\kappa_D)$, $u_D = u/\bar{u}$, $u_{pD} = u_p/\bar{u}$, $u_{eD} = u_e/\bar{u}$, $r_D = r/R$, $\kappa_D = \kappa R$, and $\omega = \bar{u}_p/\bar{u} = 1-(\bar{u}_e/\bar{u})$, in which I_0 and I_1 are the modified

Bessel functions of the first kind of order 0 and 1, u_{pD} and u_{eD} are dimensionless pressure-driven and electro-osmotic velocities, $\bar{u}$, $\bar{u}_p$, and $\bar{u}_e$ are the cross-sectional averages of the combined, pressure-driven, and electro-osmotic velocities, respectively, r_D is the dimensionless radius, κ_D is the dimensionless Debye–Hückel parameter or the dimensionless inverse of the Debye length (a measure of the dimensionless EDL thickness), and ω is the fraction of the combined flow contributed by pressure-driven (Poiseuille) flow. It should be noted that the Poiseuille contribution fraction ω is not restricted within the range of $0 \le \omega \le 1$ and it can vary from $-\infty$ to $+\infty$.[1] The case of $\omega = 1$ corresponds to the purely pressure-driven flow, whereas $\omega = 0$ refers to the case of purely EOF. In the case of $\omega \neq 0$ and $\omega \neq 1$, combined flows exist and three different scenarios may happen as described in the following:

1. For $\omega < 0$ (countercurrent flow), the pressure-driven flow ($\leftarrow$) opposes the electro-osmotic and combined flows ($\rightarrow$).
2. In the range $0 < \omega < 1$ (cocurrent flow), the pressure-driven, electro-osmotic, and combined flows have the same direction ($\rightarrow$).
3. For $\omega > 1$, (countercurrent flow) the EOF ($\leftarrow$) opposes the pressure-driven and combined flows ($\rightarrow$).

It is worth mentioning that the combined flow is always in the positive x-direction.

Chemical Species Transport. The material balance for the chemical species in the capillary tube gives the 2-D advection-diffusion equation

$$\frac{D_2}{D_1}\frac{\partial C_{1D}}{\partial t_D} + Pe\, u_D(r_D)\frac{\partial C_{1D}}{\partial x_D} = \frac{\partial^2 C_{1D}}{\partial x_D^2} + \frac{\partial^2 C_{1D}}{\partial r_D^2} + \frac{1}{r_D}\frac{\partial C_{1D}}{\partial r_D} \quad (2)$$

where $C_{1D} = C_1/C^*$, $t_D = D_2 t/R^2$, $x_D = x/R$, and $Pe = \bar{u}R/D_1$, in which C_1 is the concentration of the chemical species inside the capillary tube, C^* is the instantaneously injected chemical species concentration at time zero (as a pulse) at the inlet of the capillary tube, C_{1D} is the dimensionless chemical species concentration within the capillary tube, t is the time, D_1 is the effective molecular diffusion coefficient in the capillary tube, D_2 is the effective molecular diffusion coefficient in the porous medium, t_D is the dimensionless time, x_D is the dimensionless distance, and Pe is the Péclet number.

The mass transfer in the porous medium is assumed to be diffusion dominated. Therefore, the governing equation for chemical species transport in the porous medium can be obtained as

$$\frac{\partial^2 C_{2D}}{\partial r_D^2} + \frac{1}{r_D}\frac{\partial C_{2D}}{\partial r_D} = \frac{\partial C_{2D}}{\partial t_D} \quad (3)$$

where $C_{2D} = C_2/C^*$, in which C_2 is the chemical species concentration inside the porous medium and C_{2D} is the dimensionless chemical species concentration within the porous medium.

Equations 2 and 3 are coupled as a result of continuity of concentrations and mass fluxes along the porous wall. The appropriate initial and boundary conditions for the chemical species transport or solute in the capillary tube, Eq. 2, and the porous medium, Eq. 3, can be described as follows:

The initial chemical species concentration inside the porous medium is equal to zero

$$C_{2D}(r_D, t_D = 0) = 0 \quad (4)$$

A chemical species is injected instantaneously at time zero (as a pulse) at the inlet of the capillary tube

$$C_{1D}(x_D, r_D, t_D = 0) = \delta(x_D) \quad (5)$$

where δ is the Dirac delta function, which is equal to 1 when x_D is equal to zero and is 0 otherwise.

It is assumed that the chemical species concentration diminishes at far distance from the injection point

$$C_{1D}(x_D \to \infty, r_D, t_D) = 0 \quad (6)$$

The chemical species concentration gradient is equal to zero at the center of the capillary tube due to symmetry

$$\frac{\partial C_{1D}(x_D, r_D = 0, t_D)}{\partial r_D} = 0 \quad (7)$$

The continuity of chemical species concentrations and mass fluxes at the porous wall between the capillary tube and porous medium results in

$$C_{1D}(x_D, r_D = 1, t_D) = C_{2D}(r_D = 1, t_D) \quad (8)$$

$$D_{1D}\phi_1 \frac{\partial C_{1D}(x_D, r_D = 1, t_D)}{\partial r_D} = D_{2D}\phi_2 \frac{\partial C_{2D}(r_D = 1, t_D)}{\partial r_D} \quad (9)$$

where ϕ_1 is the porosity of the capillary tube, which is normally equal to 1, and ϕ_2 is the porosity of the porous medium. The continuity of mass fluxes at the interface between the capillary tube and the porous medium is based on Fick's first law.

There is a no-flux boundary condition at the external radius of the porous medium leading to

$$\frac{\partial C_{2D}(r_D = 1 + a, t_D)}{\partial r_D} = 0 \quad (10)$$

where $a = \Delta R/R$, in which a is the ratio of the porous medium thickness to the tube radius and ΔR is the thickness of the porous medium.

Reduction of the chemical species transport model

To reduce the 2-D solute transport model and obtain an equivalent 1-D model for advective-dispersive transport, the Reynolds decomposition method is used. In this approach the chemical species concentration and velocity in the capillary tube can be considered as the sum of the cross-sectional average values and their deviations from the averages as described by[59]

$$\begin{Bmatrix} C_{1D}(x_D, r_D, t_D) \\ u_D(r_D) \end{Bmatrix} = \begin{Bmatrix} \bar{C}_{1D}(x_D, t_D) \\ \bar{u}_D \end{Bmatrix} + \begin{Bmatrix} C'_{1D}(x_D, r_D, t_D) \\ u'_D(r_D) \end{Bmatrix} = \begin{Bmatrix} \bar{C}_{1D}(x_D, t_D) \\ 1 \end{Bmatrix} + \begin{Bmatrix} C'_{1D}(x_D, r_D, t_D) \\ u'_D(r_D) \end{Bmatrix} \quad (11)$$

where $\bar{C}_{1D}$ and $\bar{u}_D$ are the cross-sectional averages of the chemical species concentration and velocity inside the capillary tube, defined as $\int_0^1 C_{1D} 2r_D dr_D$ and $\int_0^1 u_D 2r_D dr_D = 1$, and C'_{1D} and u'_D are the corresponding deviations from the averages. From the definition of the deviations, the cross-sectional averages of deviations are zero[59]

$$\int_0^1 \left\{ \begin{array}{c} C'_{1D} \\ u'_D \end{array} \right\} 2r_D dr_D = 0 \tag{12}$$

By substitution of C_{1D} and u_D from Eq. 11 into Eqs. 2 and 4–9, one can arrive at following equations

$$\frac{D_2}{D_1}\frac{\partial \bar{C}_{1D}}{\partial t_D} + \frac{D_2}{D_1}\frac{\partial C'_{1D}}{\partial t_D} + Pe\, u_D(r_D)\frac{\partial \bar{C}_{1D}}{\partial x_D} + Pe\, u_D(r_D)\frac{\partial C'_{1D}}{\partial x_D} = \frac{\partial^2 \bar{C}_{1D}}{\partial x_D^2} + \frac{\partial^2 C'_{1D}}{\partial x_D^2} + \frac{\partial^2 C'_{1D}}{\partial r_D^2} + \frac{1}{r_D}\frac{\partial C'_{1D}}{\partial r_D} \tag{13}$$

$$\bar{C}_{1D}(x_D, t_D=0) + C'_{1D}(x_D, r_D, t_D=0) = \delta(x_D) \tag{14}$$

$$\bar{C}_{1D}(x_D \to \infty, t_D) + C'_{1D}(x_D \to \infty, r_D, t_D) = 0 \tag{15}$$

$$\frac{\partial C'_{1D}(x_D, r_D=0, t_D)}{\partial r_D} = 0 \tag{16}$$

$$\bar{C}_{1D}(x_D, t_D) + C'_{1D}(x_D, r_D=1, t_D) = C_{2D}(r_D=1, t_D) \tag{17}$$

$$D_{1D}\phi_1 \frac{\partial C'_{1D}(x_D, r_D=1, t_D)}{\partial r_D} = D_{2D}\phi_2 \frac{\partial C_{2D}(r_D=1, t_D)}{\partial r_D} \tag{18}$$

Taking the cross-sectional average of Eq. 13 and using Eqs. 12 and 16 result in

$$\frac{D_2}{D_1}\frac{\partial \bar{C}_{1D}}{\partial t_D} + Pe\,\frac{\partial \bar{C}_{1D}}{\partial x_D} + Pe\,\overline{u_D(r_D)\frac{\partial C'_{1D}}{\partial x_D}} = \frac{\partial^2 \bar{C}_{1D}}{\partial x_D^2} + 2\frac{\partial C'_{1D}(x_D, r_D=1, t_D)}{\partial r_D} \tag{19}$$

By introducing a new dimensionless parameter, β, Eq. 19 can be generalized to incorporate impervious (or no-flux) boundary condition at the wall of the capillary tube as given by

$$\frac{D_2}{D_1}\frac{\partial \bar{C}_{1D}}{\partial t_D} + Pe\,\frac{\partial \bar{C}_{1D}}{\partial x_D} + Pe\,\overline{u_D(r_D)\frac{\partial C'_{1D}}{\partial x_D}} = \frac{\partial^2 \bar{C}_{1D}}{\partial x_D^2} + 2\beta\frac{\partial C'_{1D}(x_D, r_D=1, t_D)}{\partial r_D} \tag{20}$$

where

$$\beta = \begin{cases} 0 & \text{Tube with impervious wall (or noncoupled system)} \\ 1 & \text{Tube with porous wall (or coupled system)} \end{cases} \tag{21}$$

Subtracting Eq. 20 from Eq. 13 leads to

$$\frac{D_2}{D_1}\frac{\partial C'_{1D}}{\partial t_D} + Pe\,[u_D(r_D)-1]\frac{\partial \bar{C}_{1D}}{\partial x_D} + Pe\,u_D(r_D)\frac{\partial C'_{1D}}{\partial x_D} - Pe\,\overline{u_D(r_D)\frac{\partial C'_{1D}}{\partial x_D}} = \frac{\partial^2 C'_{1D}}{\partial x_D^2} + \frac{\partial^2 C'_{1D}}{\partial r_D^2} + \frac{1}{r_D}\frac{\partial C'_{1D}}{\partial r_D} - 2\beta\frac{\partial C'_{1D}(x_D, r_D=1, t_D)}{\partial r_D} \tag{22}$$

To this point Eq. 22 is exact. Now, we use three important assumptions adopted from Taylor[17] and Fischer et al.[62] on the theory of dispersive solute transport for determination of a dispersion coefficient. Based on Taylor's theory, after a sufficient time has elapsed as the introduction of solute into the capillary tube, transverse diffusion eliminates concentration deviations in the transverse direction and, thus, a quasi steady-state condition can be reached implying that $\partial C'_{1D}/\partial t_D \approx 0$. In other words, for a time scale on the order of the diffusion time across the capillary tube, $\tau = R^2/D_1$, the process has reached the condition that no appreciable transverse concentration deviations exist.[17,24,26,62,63] Also, the deviation of concentration in the capillary tube, C'_{1D}, is a slowly varying function and, therefore, the third and fourth terms on the left-hand side of Eq. 22 will nearly balance each other.[62] In addition, longitudinal advection can be considered to be dominant as compared with longitudinal diffusion ($Pe\,[u_D(r_D)-1]\partial \bar{C}_{1D}/\partial x_D \gg \partial^2 C'_{1D}/\partial x_D^2$). This assumption recognizes that longitudinal transport of solute is mainly due to longitudinal advection and longitudinal diffusion does not play any role.[17,24,26,62,64] By taking into consideration these assumptions and using Eq. 1 and making some rearrangements, Eq. 22 reduces to

$$\left(2\omega(1-r_D^2) + f_e(1-\omega)\left[1-\frac{I_0(\kappa_D r_D)}{I_0(\kappa_D)}\right]-1\right)Pe\frac{\partial \bar{C}_{1D}}{\partial x_D} + 2\beta\frac{\partial C'_{1D}(x_D, r_D=1, t_D)}{\partial r_D} = \frac{1}{r_D}\frac{\partial}{\partial r_D}\left[r_D\frac{\partial C'_{1D}}{\partial r_D}\right] \tag{23}$$

To obtain C'_{1D}, it is needed to integrate both sides of Eq. 23 with respect to r_D twice and use Eqs. 12 and 16 to determine constants of integration, which gives

$$C'_{1D} = \left[-\frac{1}{8}\omega r_D^4 + \frac{1}{4}[2\omega-1+f_e(1-\omega)]r_D^2 - f_e(1-\omega)\frac{I_0(\kappa_D r_D)}{\kappa_D^2 I_0(\kappa_D)} + \frac{1}{8} - \frac{5}{24}\omega - \frac{f_e(1-\omega)}{\kappa_D^2}\left(\frac{1}{f_e}+\frac{\kappa_D^2}{8}-1\right)\right]Pe\frac{\partial \bar{C}_{1D}}{\partial x_D} - \frac{\beta}{4}\frac{\partial C'_{1D}(x_D, r_D=1, t_D)}{\partial r_D}(1-2r_D^2) \tag{24}$$

To close the formulation, it is required to find the term $\overline{u_D(r_D)\partial C'_{1D}/\partial x_D}$ in Eq. 20. The first derivative of Eq. 24 with respect to x_D is obtained as follows

$$\frac{\partial C'_{1D}}{\partial x_D} = \left[-\frac{1}{8}\omega r_D^4 + \frac{1}{4}[2\omega-1+f_e(1-\omega)]r_D^2 - f_e(1-\omega)\frac{I_0(\kappa_D r_D)}{\kappa_D^2 I_0(\kappa_D)} + \frac{1}{8} - \frac{5}{24}\omega - \frac{f_e(1-\omega)}{\kappa_D^2}\left(\frac{1}{f_e}+\frac{\kappa_D^2}{8}-1\right)\right]Pe\frac{\partial^2 \bar{C}_{1D}}{\partial x_D^2} - \frac{\beta}{4}\frac{\partial^2 C'_{1D}(x_D, r_D=1, t_D)}{\partial r_D \partial x_D}(1-2r_D^2) \tag{25}$$

By Eqs. 1 and 25, the cross-sectional average of $u_D(r_D)\partial C'_{1D}/\partial x_D$ is derived as

$$\overline{u_D(r_D)\frac{\partial C'_{1D}}{\partial x_D}} = \int_0^1 \left(u_D(r_D)\frac{\partial C'_{1D}}{\partial x_D}\right)2r_D dr_D = [Y_{p1}\omega^2 + Y_{p2}\omega + Y_{pe}\omega(1-\omega) + Y_{e1}(1-\omega)^2 + Y_{e2}(1-\omega)]Pe\frac{\partial^2 \bar{C}_{1D}}{\partial x_D^2} + 2\beta[-Y_{p2}\omega - Y_{e2}(1-\omega)]\frac{\partial^2 C'_{1D}(x_D, r_D=1, t_D)}{\partial r_D \partial x_D} \tag{26}$$

where $Y_{p1} = -1/16$, $Y_{p2} = 1/24$, and

$$Y_{pe} = f_e\left[-\frac{1}{24}(1+8\lambda) + \frac{(1+2\lambda)}{\kappa_D^2} - \frac{16(1-2\lambda)}{\kappa_D^4}\right] \tag{27}$$

$$Y_{e1}=f_e^2\left[-\frac{1}{4}(\lambda+4\lambda^2)+\frac{2(1-\lambda-2\lambda^2)}{\kappa_D^2}\right] \tag{28}$$

$$Y_{e2}=f_e\left[\frac{1}{4}\lambda-\frac{(1-2\lambda)}{\kappa_D^2}\right] \tag{29}$$

The integration indicated in Eq. 26 is lengthy but straightforward, although it may be tedious due to involving the Lommel[65] and other difficult integrals.[65] Appendix A shows these integrals accompanied with the modified Bessel functions of the first kind of order 2 and 3 (I_2, I_3) as functions of the modified Bessel functions of the first kind of order 0 and 1 (I_0, I_1).[65]

Combination of Eqs. 20 and 26 and making some rearrangements result in

$$\begin{aligned}&\frac{D_2}{D_1}\frac{\partial\bar{C}_{1D}}{\partial t_D}+Pe\frac{\partial\bar{C}_{1D}}{\partial x_D}=\\&[1-[Y_{p1}\,\omega^2+Y_{p2}\,\omega+Y_{pe}\,\omega\,(1-\omega)+Y_{e1}\,(1-\omega)^2\\&+Y_{e2}\,(1-\omega)]Pe^2]\frac{\partial^2\bar{C}_{1D}}{\partial x_D^2}+2\beta\frac{\partial C'_{1D}(x_D,r_D=1,t_D)}{\partial r_D}\\&+2\beta\,[Y_{p2}\,\omega+Y_{e2}\,(1-\omega)]\,Pe\frac{\partial^2C'_{1D}(x_D,r_D=1,t_D)}{\partial r_D\partial x_D}\end{aligned} \tag{30}$$

To eliminate $\partial C'_{1D}(x_D,r_D=1,t_D)/\partial r_D$ in Eq. 30, Eq. 24 is used for $r_D=1$ and $\beta=1$ and then it is combined with Eq. 17, which gives

$$\begin{aligned}\frac{\partial C'_{1D}(x_D,r_D=1,t_D)}{\partial r_D}&=4C_{2D}(r_D=1,t_D)-4\bar{C}_{1D}\\&-\left[-\frac{1}{2}+Y_{p3}\,\omega+Y_{e3}\,(1-\omega)\right]Pe\frac{\partial\bar{C}_{1D}}{\partial x_D}\end{aligned} \tag{31}$$

where $Y_{p3}=2/3$ and

$$Y_{e3}=f_e\left[\frac{1}{2}-\frac{4(1-2\lambda)}{\kappa_D^2}\right] \tag{32}$$

Also, for elimination of the term $\partial^2C'_{1D}(x_D,r_D=1,t_D)/\partial r_D\,\partial x_D$ in Eq. 30, Eq. 25 is applied for $r_D=1$ and $\beta=1$ and then it is combined with the first derivative of Eq. 17 with respect to x_D, which results in

$$\begin{aligned}\frac{\partial^2C'_{1D}(x_D,r_D=1,t_D)}{\partial r_D\partial x_D}&=-4\frac{\partial\bar{C}_{1D}}{\partial x_D}\\&-\left[-\frac{1}{2}+Y_{p3}\,\omega+Y_{e3}\,(1-\omega)\right]Pe\frac{\partial^2\bar{C}_{1D}}{\partial x_D^2}\end{aligned} \tag{33}$$

By considering $\beta=1$, which resembles a coupled system, and combination of Eqs. 30, 31, and 33 and making some rearrangements, one gets

$$\begin{aligned}&\frac{D_2}{D_1}\frac{\partial\bar{C}_{1D}}{\partial t_D}+[Z_p\,\omega+Z_e\,(1-\omega)]\,Pe\frac{\partial\bar{C}_{1D}}{\partial x_D}=\\&[1-[X_p\,\omega^2+X_{pe}\,\omega\,(1-\omega)+X_e\,(1-\omega)^2]Pe^2]\frac{\partial^2\bar{C}_{1D}}{\partial x_D^2}\\&+8[C_{2D}(r_D=1,t_D)-\bar{C}_{1D}]\end{aligned} \tag{34}$$

where $Z_p=8Y_{p2}+2Y_{p3}=5/3$, $X_p=Y_{p1}+2Y_{p2}Y_{p3}=-1/144$, and

$$X_{pe}=Y_{pe}+2Y_{p2}Y_{e3}+2Y_{e2}Y_{p3}=f_e\left[-\frac{2}{3}\frac{(1-8\lambda)}{\kappa_D^2}-\frac{16(1-2\lambda)}{\kappa_D^4}\right] \tag{35}$$

$$X_e=Y_{e1}+2Y_{e2}Y_{e3}=f_e^2\left[-\lambda^2+\frac{(1-2\lambda)}{\kappa_D^2}+\frac{8(1-4\lambda+4\lambda^2)}{\kappa_D^4}\right] \tag{36}$$

$$Z_e=8Y_{e2}+2Y_{e3}=f_e\left[(1+2\lambda)-\frac{16(1-2\lambda)}{\kappa_D^2}\right] \tag{37}$$

Equation 34 shows an equivalent 1-D model for advective-dispersive transport in the capillary tube, in which the interaction between the capillary tube and porous medium is handled by imposing the continuity of concentrations and mass fluxes at the porous wall. The coefficients of $\partial\bar{C}_{1D}/\partial x_D$ and $\partial^2\bar{C}_{1D}/\partial x_D^2$ in Eq. 34 show the equivalent average velocity and the dispersion coefficient, respectively, in a coupled system.

To solve Eq. 34, the appropriate initial and boundary conditions can be obtained by taking the cross-sectional average of Eqs. 14 and 15 and using Eq. 12, which result in

$$\bar{C}_{1D}(x_D,t_D=0)=\delta(x_D) \tag{38}$$

$$\bar{C}_{1D}(x_D\to\infty,t_D)=0 \tag{39}$$

The suitable initial and boundary conditions for solving Eq. 3, which is the governing equation for transport of chemical species in the porous medium, are as follows

$$C_{2D}(r_D,t_D=0)=0 \tag{40}$$

$$\begin{aligned}C_{2D}(r_D=1,t_D)-\frac{1}{4}\frac{D_2}{D_1}\frac{\phi_2}{\phi_1}\frac{\partial C_{2D}(r_D=1,t_D)}{\partial r_D}&=\bar{C}_{1D}\\&+\left[-\frac{1}{2}+Y_{p3}\,\omega+Y_{e3}\,(1-\omega)\right]\frac{Pe}{4}\frac{\partial\bar{C}_{1D}}{\partial x_D}\end{aligned} \tag{41}$$

$$\frac{\partial C_{2D}(r_D=1+a,t_D)}{\partial r_D}=0 \tag{42}$$

where Eq. 41 can be obtained by combination of Eqs. 18 and 31.

The Laplace transform method can be applied to solve Eqs. 3 and 34 and find the average concentrations in both domains and mass of the chemical species delivered to the porous medium surrounding the capillary tube. Here our focus is on dispersion coefficient due to a combined pressure-driven and EOF in a capillary tube with a porous wall (or coupled system).

Dispersion coefficient in a noncoupled system

The deviation of the combined velocity profile from its cross-sectional average gives rise to the dispersion in a capillary tube with an impervious wall (or a noncoupled system). Using the definition of the Péclet number, the dimensionless dispersion coefficient of chemical species for a noncoupled system ($\hat{\mathbf{D}}_{\text{noncoupled}}=\mathbf{D}_{\text{noncoupled}}/D_1$) can be obtained using $\beta=0$ in Eq. 30

$$\begin{aligned}\hat{\mathbf{D}}_{\text{noncoupled}}=1-[&Y_{p1}\,\omega^2+Y_{p2}\,\omega+Y_{pe}\,\omega\,(1-\omega)\\&+Y_{e1}\,(1-\omega)^2+Y_{e2}\,(1-\omega)]Pe^2\end{aligned} \tag{43}$$

Datta and Kotamarthi[1] applied a different approach and presented a dispersion coefficient in a noncoupled system (or a capillary tube with a nonporous wall) for the case of sufficiently low wall or zeta potential that accounts for the combined flows. It is worth noting that one can find an excellent agreement between our results and those presented by Datta and Kotamarthi.[1] This comparison can be made here for validation of our model.

The two factors Y_{p1} and Y_{p2} in Eq. 43 are constant and as it is clear from Eqs. 27–29, the three factors Y_{pe}, Y_{e1}, and Y_{e2} in Eq. 43 depend on the dimensionless Debye–Hückel parameter, $\kappa_D = \kappa R$. For this study, the range of the dimensionless Debye–Hückel parameter is taken as $1 \leq \kappa_D \leq 100$. These values are commonly reported in the literature for typical applications of EOFs.[12–14,66] In the limit of a very thin EDL $(\kappa_D \rightarrow +\infty)$ Eq. 43 can be simplified as follows

$$\lim_{\kappa_D \rightarrow +\infty} \left\{ Y_{p1},\, Y_{p2},\, Y_{pe},\, Y_{e1},\, Y_{e2} \right\} = \left\{ -\frac{1}{16}, \frac{1}{24}, -\frac{1}{24}, 0, 0 \right\}$$
$$\rightarrow \qquad \lim_{\kappa_D \rightarrow +\infty} \hat{\mathbf{D}}_{\text{noncoupled}} = 1 + \frac{1}{48} (\omega Pe)^2 \tag{44}$$

For the case of pressure-driven (Poiseuille) flow, $\omega = 1$, with a parabolic velocity profile, Eq. 44 turns to the dispersion coefficient in a noncoupled system presented by Taylor.[17]

Dispersion coefficient in a coupled system

The deviation of the combined velocity profile from its cross-sectional average and the interaction between the fluids inside the capillary tube and the porous medium can affect the dispersion in a capillary tube with a porous wall (or a coupled system), which is the main purpose of this study and will be discussed shortly. The dimensionless dispersion coefficient for a coupled system ($\hat{\mathbf{D}}_{\text{coupled}} = \mathbf{D}_{\text{coupled}} / D_1$) can be obtained using Eq. 34

$$\hat{\mathbf{D}}_{\text{coupled}} = 1 - [X_p\, \omega^2 + X_{pe}\, \omega\, (1-\omega) + X_{\text{e}}\, (1-\omega)^2] Pe^2 \tag{45}$$

The first term on the right-hand side of the noncoupled and coupled dispersion coefficients, Eqs. 43 and 45, represents the dispersion due to molecular diffusion. The other terms on the right-hand side of these equations are caused by combination of transverse diffusion and longitudinal advection (i.e., shear or Taylor dispersion).

The factor X_p in Eq. 45 is constant and as it is clear from Eqs. 35 and 36, the two factors X_{pe} and X_e in Eq. 45 depend on the ratio of the tube radius to the Debye length. Under the condition of a very thin EDL $(\kappa_D \rightarrow +\infty)$, Eq. 45 can be reduced to

$$\lim_{\kappa_D \rightarrow +\infty} \left\{ X_p,\, X_{pe},\, X_{\text{e}} \right\} = \left\{ -\frac{1}{144}, 0, 0 \right\}$$
$$\rightarrow \qquad \lim_{\kappa_D \rightarrow +\infty} \hat{\mathbf{D}}_{\text{coupled}} = 1 + \frac{1}{144} (\omega Pe)^2 \tag{46}$$

For the case of $\omega = 1$, which corresponds to purely pressure-driven flow, Eq. 46 is simplified to the coupled dispersion coefficient recently developed by Dejam et al.[32]

By defining the ratio of the dispersion coefficients in the coupled and noncoupled systems as $R_{\mathbf{D}} = \hat{\mathbf{D}}_{\text{coupled}} / \hat{\mathbf{D}}_{\text{noncoupled}}$ and using Eqs. 44 and 46, one can arrive at

$$\lim R_{\mathbf{D}\, \kappa_D \rightarrow +\infty} = \frac{1 + \frac{1}{144} (\omega Pe)^2}{1 + \frac{1}{48} (\omega Pe)^2} \tag{47}$$

In the limit of a very high Péclet number $Pe \rightarrow +\infty$, Eq. 47 reduces to $R_{\mathbf{D}} = 1/3$, which was reported recently by Dejam et al.[32] for the case of purely pressure-driven flow.

Results and Discussion

In the following subsections, the effects of Péclet number, Debye–Hückel parameter, and Poiseuille contribution fraction on dispersion coefficient in a coupled system are studied and compared with the one obtained for the noncoupled system.

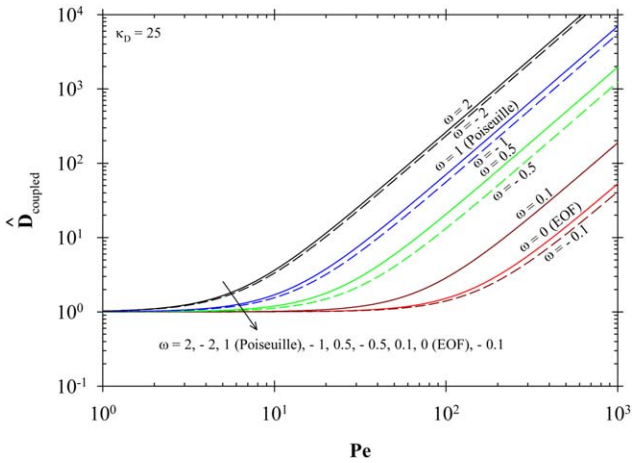

Figure 2. Dimensionless dispersion coefficient in a coupled system vs. Péclet number for a variety of the Poiseuille contribution fractions when $\kappa_D = 25$.

[Color figure can be viewed in the online issue, which is available at wileyonlinelibrary.com.]

The effect of Péclet number

Figure 2 demonstrates the dimensionless dispersion coefficient in a coupled system vs. Péclet number for different ω and $\kappa_D = 25$. As may be expected, the coupled dispersion coefficient for the purely EOF ($\omega = 0$) is considerably smaller than the one for the case of purely pressure-driven flow ($\omega = 1$). Results show that for $0 < \omega < 1$ (scenario ii), the coupled dispersion coefficient is between those for $\omega = 0$ and $\omega = 1$. When $-1 \leq \omega < 0$ (scenario i), values of the coupled dispersion coefficient are less than those for purely pressure-driven flow. For $\omega = -0.1$ (scenario i), values of the coupled dispersion coefficient are even smaller than the case of purely EOF, which indicates that the coupled dispersion coefficient can be further reduced in the presence of small countercurrent pressure-driven flow with a negative Poiseuille contribution fraction close to zero. When $|\omega| > 1$ (scenarios i and iii), the coupled dispersion coefficient is observed to be greater than that for purely pressure-driven flow. Figure 2 reveals that the coupled dispersion coefficient for $-\omega$ is generally smaller than that for $+\omega$. However, by increasing the absolute value of the Poiseuille contribution fraction, the coupled dispersion coefficients for ω and $-\omega$ become closer and finally approach each other when $\omega \rightarrow \pm\infty$. The analytical formula, expressing this condition, can be obtained using Eq. 45

$$\lim_{\omega \rightarrow \pm\infty} \hat{\mathbf{D}}_{\text{coupled}} = (X_{pe} - X_p - X_{\text{e}})\, (\omega Pe)^2 \tag{48}$$

which turns to $\lim \hat{\mathbf{D}}_{\text{coupled}_{\omega \rightarrow \pm\infty}} = 0.00616\, (\omega Pe)^2$ as $X_{pe} - X_p - X_{\text{e}} = 0.00616$ for $\kappa_D = 25$.

The results illustrated in Figure 2 show that as expected three regimes can be identified: diffusion-dominated, transition, and advection-dominated regimes. The required Péclet number for transition to the advection-dominated regime for $\omega > 0$ (scenarios ii and iii) is generally smaller than that for $\omega < 0$ (scenario i).

Figure 3 shows the ratio of the dispersion coefficients in the coupled and noncoupled systems vs. Péclet number for $\omega = 0$,

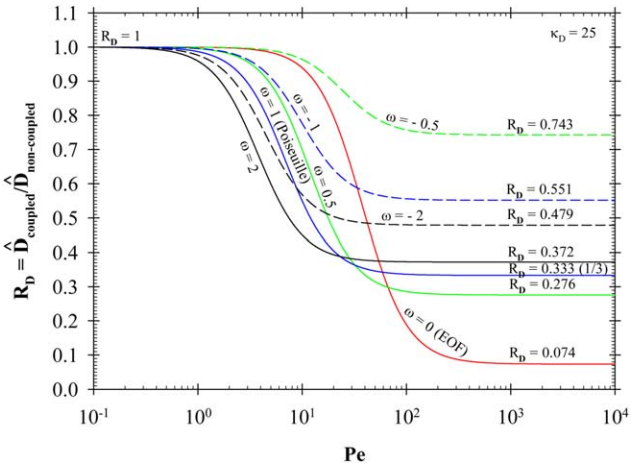

Figure 3. The ratio of the dispersion coefficient in a coupled system to the dispersion coefficient in a noncoupled system vs. Péclet number for $\omega = 0$, ± 0.5, ± 1, ± 2, and $\kappa_D = 25$ using Eqs. 43 and 45.

[Color figure can be viewed in the online issue, which is available at wileyonlinelibrary.com.]

± 0.5, ± 1, ± 2, and $\kappa_D = 25$ using Eqs. 43 and 45. This plot also more clearly identifies three different regimes of diffusion-dominated, transition, and advection-dominated. The ratio is unity for small Péclet numbers in the first regime where the dispersion does not play an important role in transport of chemical species. The ratio is a function of the Péclet number in the middle regime and it varies within the range $\lim R_{\mathbf{D}Pe\to+\infty} < R_{\mathbf{D}} < 1$, in which the lower limit can be obtained for each value of ω using Eqs. 43 and 45

$$\lim_{Pe\to+\infty} R_{\mathbf{D}} = \frac{X_p\,\omega^2 + X_{pe}\,\omega\,(1-\omega) + X_e\,(1-\omega)^2}{Y_{p1}\,\omega^2 + Y_{p2}\,\omega + Y_{pe}\,\omega\,(1-\omega) + Y_{e1}\,(1-\omega)^2 + Y_{e2}\,(1-\omega)} \tag{49}$$

The right-hand side of Eq. 49 is calculated as 0.074, 0.276, 0.743, 0.333 (1/3), 0.551, 0.372, and 0.479 for $\omega = 0$, 0.5, -0.5, 1, -1, 2, and -2, respectively, for $\kappa_D = 25$. The coupled dispersion coefficient is $R_{\mathbf{D}}$ times smaller than the noncoupled dispersion coefficient for high Péclet numbers in the third regime. The presented results illustrate that it is essential to include the species transport between the capillary tube and the surrounding porous medium in development of the dispersion coefficient for the last two regimes. A detailed description of the three aforementioned regimes for the case of the pressure-driven flow, $\omega = 1$, can be found elsewhere.[31,32] When $\omega \to \pm\infty$, Eq. 49 reduces to

$$\lim_{Pe\to+\infty,\ \ \omega\to\pm\infty} R_{\mathbf{D}} = \frac{X_p - X_{pe} + X_e}{Y_{p1} - Y_{pe} + Y_{e1}} \tag{50}$$

which turns to $\lim R_{\mathbf{D}Pe\to+\infty,\ \ \omega\to\pm\infty} = 0.420$ as $X_p - X_{pe} + X_e = -0.00616$ and $Y_{p1} - Y_{pe} + Y_{e1} = -0.01468$ for $\kappa_D = 25$.

The coupled dispersion coefficients described by Eq. 45 are plotted vs. Péclet number in Figure 4 for several values of the dimensionless Debye–Hückel parameter. In Figures 4a, b $\omega$is taken as -3.5 and -0.5 (countercurrent), which refer to the scenario i, in Figure 4c ω is taken as 0.5 (cocurrent), which corresponds to the scenario ii, and in Figure 4d ω is taken as 1.5 (countercurrent), which corresponds to the scenario iii. Results shown in Figures 4c, d reveal that the coupled dispersion coefficient demonstrates a monotonic behavior with respect to κ_D for flows with characteristics of scenarios ii and iii. However, it behaves nonmonotonically for scenario i with $\omega = -0.5$ as shown in Figure 4b. It is worth noting that the behavior of the coupled dispersion coefficient terns monotonic by further decrease of ω as depicted in Figure 4a. Furthermore, results indicate that for both cocurrent and countercurrent flows for $\kappa_D > 50$ the coupled dispersion coefficients remain constant by increasing κ_D, which resembles the same velocity profile for large values of κ_D. The combined velocity profile can be obtained for any values of the Poiseuille contribution fraction in the limit of a very thin EDL ($\kappa_D \to +\infty$) using Eq. 1 as $\lim u_D(r_D)_{\kappa_D\to+\infty} = 1 + \omega\,(1 - 2r_D^2)$. The coupled dispersion coefficients for cocurrent and countercurrent flows at large κ_D can be obtained by applying Eq. 45. It is worth noting that the combined velocity profiles are different for each values of the $\omega = \pm 0.5$ under the condition of a very thin EDL when $\kappa_D \to +\infty$ while the coupled dispersion coefficients are the same (see Figures 4b, c).

The effect of Debye–Hückel parameter

Figure 5 illustrates the dimensionless dispersion coefficient in a coupled system vs. dimensionless Debye–Hückel parameter, for a variety of the Poiseuille contribution fractions and $Pe = 50$ using Eq. 45. As expected, for the case of purely pressure-driven flow ($\omega = 1$) the coupled dispersion coefficient is independent of the Debye length and it is noticeably larger than that for the case of purely EOF ($\omega = 0$). For a constant value of ω within the ranges $-1 \le \omega < 0$ (scenario i) and $0 < \omega < 1$ (scenario ii), the coupled dispersion coefficient gives values that are generally between those of $\omega = 0$ and $\omega = 1$. In general, for large κ_D the coupled dispersion coefficient is seen to be greater than that of $\omega = 1$ when $|\omega| > 1$ (scenarios i and iii). Figure 5 reveals that the coupled dispersion coefficient for $-\omega$ is smaller than that for ω. However, as the dimensionless Debye–Hückel parameter increases, the coupled dispersion coefficients for ω and $-\omega$ become closer and finally approach each other in the limit of a very thin EDL ($\kappa_D \to +\infty$). Equation 45, which is used to express this condition, turns to $\lim \hat{\mathbf{D}}_{\text{coupled}_{\kappa_D\to+\infty}} = 1$, 5.340, 18.361, and 70.444 for $\omega = 0$, ± 0.5, ± 1, and ± 2, respectively, at $Pe = 50$.

Figure 6 shows the ratio of the dispersion coefficients in the coupled and noncoupled systems vs. dimensionless Debye–Hückel parameter for $\omega = 0$, ± 0.5, ± 1, ± 2, and $Pe = 50$ using Eqs. 43 and 45. The variation of this ratio for $\omega \le 0$ (purely electro-osmotic and scenario i) is much larger than that for $\omega > 0$ (purely pressure-driven and flows with characteristics of scenarios ii and iii). However, by increasing the dimensionless Debye–Hückel parameter, the coupled dispersion coefficients for ω and $-\omega$ become closer and ultimately approach each other in the limit of a very thin EDL ($\kappa_D \to +\infty$). At this condition, Eq. 47 turns to $\lim R_{\mathbf{D}\ \kappa_D\to+\infty} = 1$, 0.381, 0.346, and 0.336 for $\omega = 0$, ± 0.5, ± 1, and ± 2, respectively, at $Pe = 50$.

The results shown in Figure 6 also reveal that consideration of the mass transfer between the capillary tube and porous medium for $\omega > 0$ is much important than that for $\omega \le 0$. Also, for the application of interest with combined flows, in which a very thin EDL $\kappa^{-1} \to 0$ exists, inclusion of the mass transport from the tube to the porous medium is necessary regardless of the value used for the Poiseuille contribution fraction.

The coupled dispersion coefficients described by Eq. 45 are plotted vs. dimensionless Debye–Hückel parameter in Figure 7

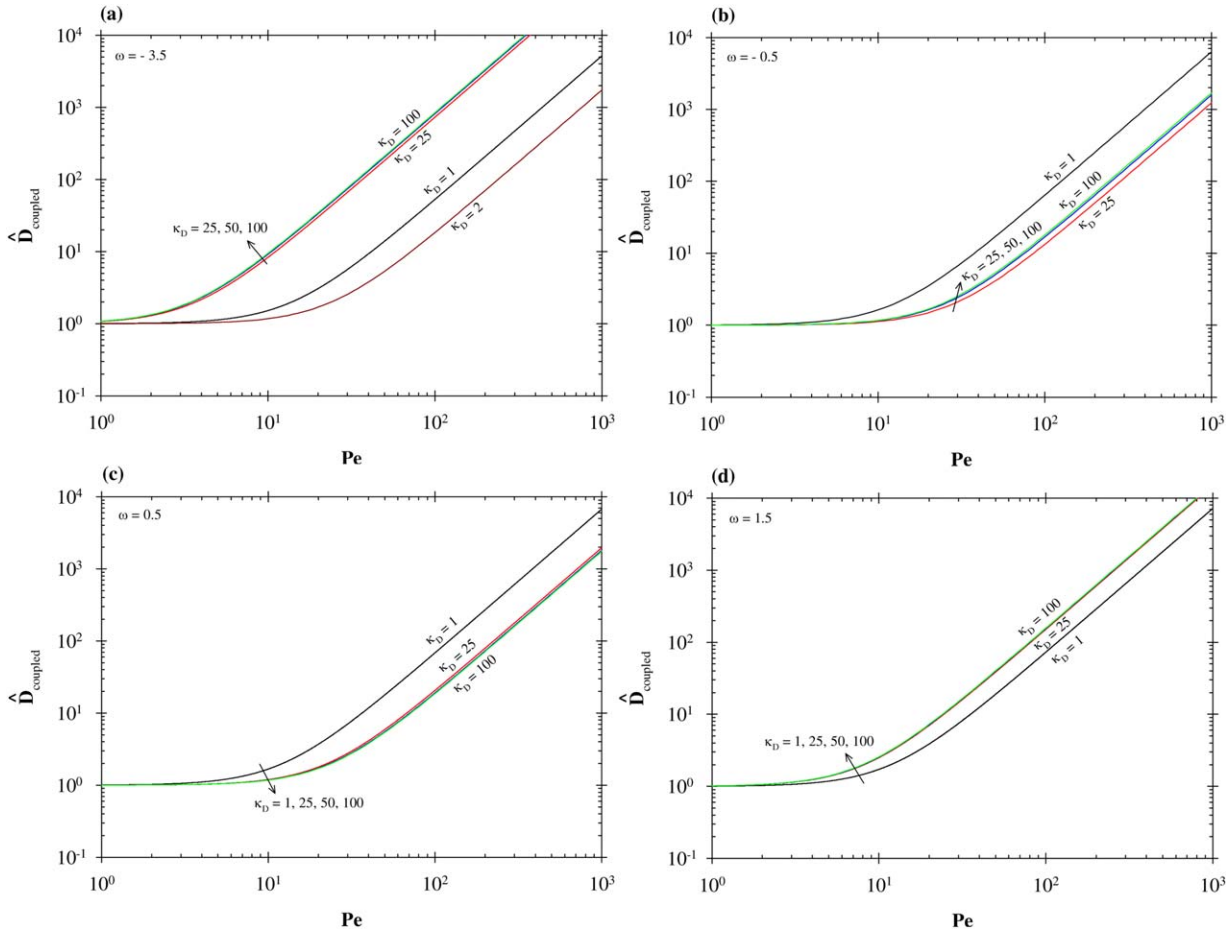

Figure 4. The coupled dispersion coefficients vs. Péclet number for different values of the dimensionless Debye–Hückel parameter: (a) $\omega = -3.5$, (b) $\omega = -0.5$, (c) $\omega = 0.5$, and (d) $\omega = 1.5$.

[Color figure can be viewed in the online issue, which is available at wileyonlinelibrary.com.]

for several values of the Péclet number. In Figures 11a–d, ω is taken as -3.5 (scenario i), -0.5 (scenario i), 0.5 (scenario ii), and 1.5 (scenario iii), respectively. For $\omega = -3.5$ and $\omega = -0.5$ (Figures 11a, b), $\hat{\mathbf{D}}_{\text{coupled}}$ is almost equal to 1 for low Péclet numbers whereas it shows a minimum around $\kappa_D = 3$ for $\omega = -3.5$ and $\kappa_D = 8$ for $\omega = -0.5$ in the case of high Péclet numbers. For $\omega = 0.5$ (Figure 11c), $\hat{\mathbf{D}}_{\text{coupled}}$ is almost unity in

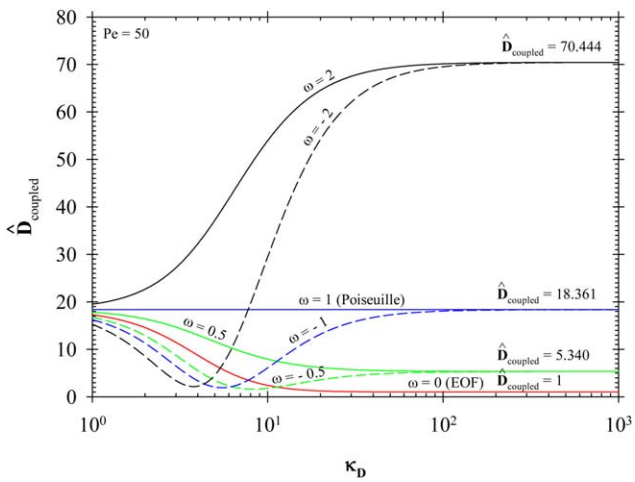

Figure 5. Dimensionless dispersion coefficient in a coupled system vs. dimensionless Debye–Hückel parameter for various ω and $Pe = 50$.

[Color figure can be viewed in the online issue, which is available at wileyonlinelibrary.com.]

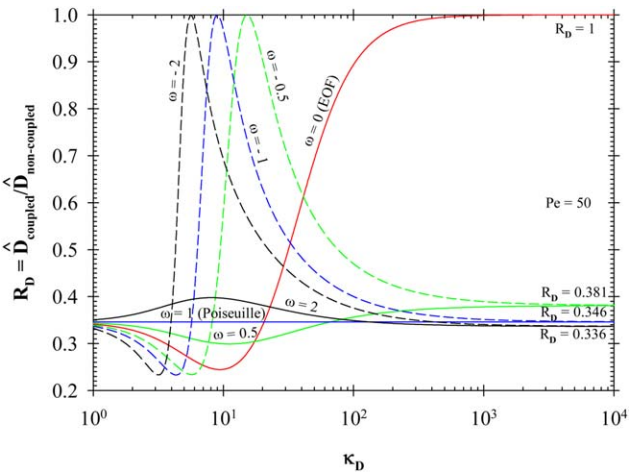

Figure 6. The ratio of the dispersion coefficient in a coupled system to the dispersion coefficient in a noncoupled system vs. dimensionless Debye–Hückel parameter for $\omega = 0, \pm 0.5, \pm 1, \pm 2$, and $Pe = 50$ using Eqs. 43 and 45.

[Color figure can be viewed in the online issue, which is available at wileyonlinelibrary.com.]

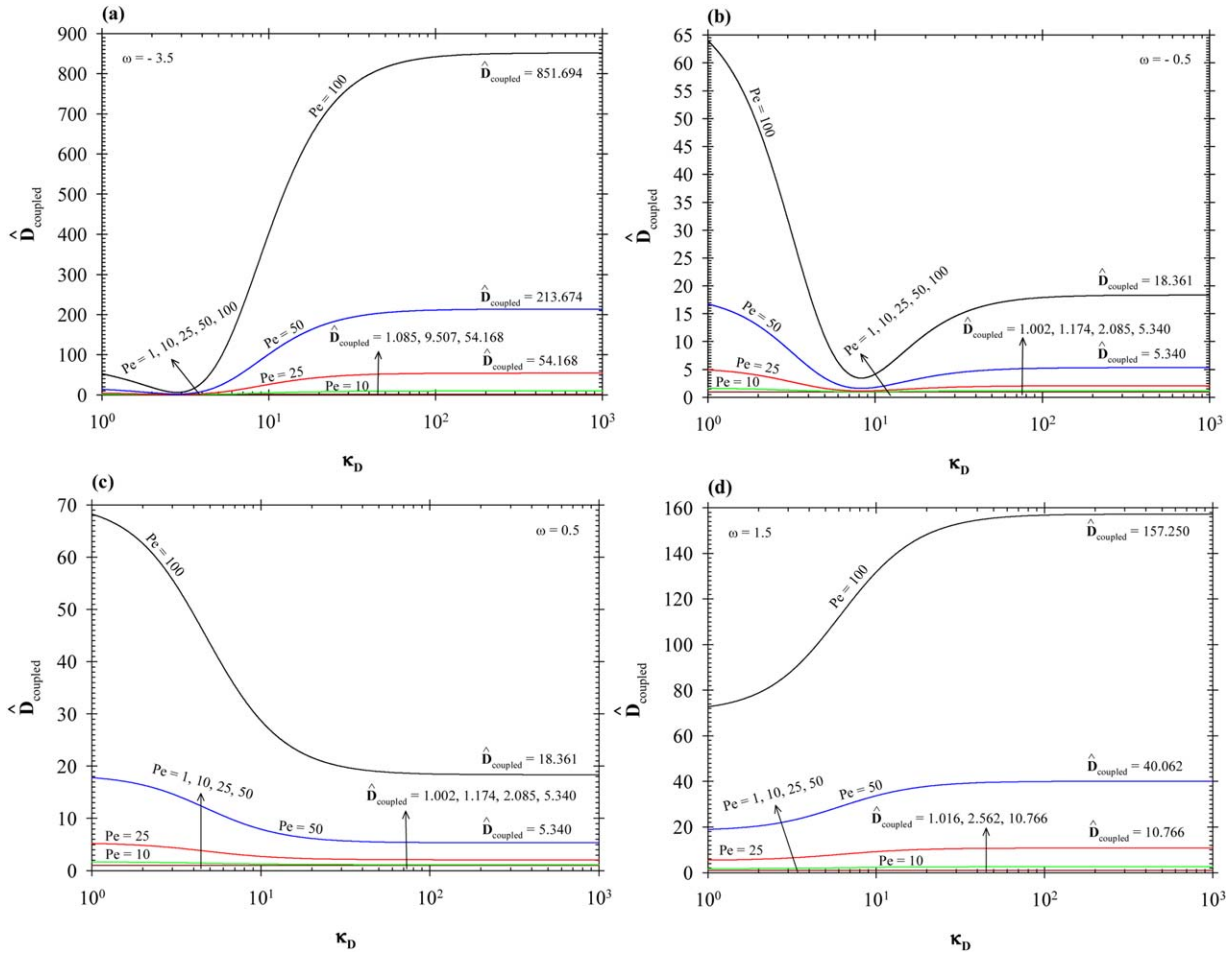

Figure 7. The coupled dispersion coefficients vs. dimensionless Debye–Hückel parameter for different values of the Péclet number: (a) $\omega = -3.5$, (b) $\omega = -0.5$, (c) $\omega = 0.5$, and (d) $\omega = 1.5$.

[Color figure can be viewed in the online issue, which is available at wileyonlinelibrary.com.]

the case of low Péclet numbers ($Pe < 10$) while in the case of relatively high Péclet numbers ($Pe > 25$) it decreases first and then remains constant by increasing the dimensionless Debye–Hückel parameter. However, for both values of $\omega = \pm 0.5$ the coupled dispersion coefficient remains constant in the limit of a very thin EDL $\kappa_D \to +\infty$. For $\omega = 1.5$ (Figure 11d), $\hat{\mathbf{D}}_{\text{coupled}}$ is almost unity in the case of low Péclet numbers while in the case of relatively high Péclet numbers it increases first and then remains constant by increasing the dimensionless Debye–Hückel parameter. Calculation of the coupled dispersion coefficient involves evaluation of $I_1(\kappa_D)/I_0(\kappa_D)$, which approaches infinity for large values of $\kappa_D > 709.7$. Appendix B shows implementation of this ratio to avoid this problem.[21,67]

The effect of Poiseuille contribution fraction

Figure 8 shows the dimensionless dispersion coefficient in a coupled system vs. Poiseuille contribution fraction for a number of the dimensionless Debye–Hückel parameters and $Pe = 50$ using Eq. 45. For a constant value of the Debye length the dimensionless dispersion coefficient vs. ω shows a minimum. As shown in Figure 8, for large absolute values of ω, the dimensionless dispersion coefficient can be considerably greater than 1. The Poiseuille contribution fraction that results in minimum dispersion, $(\omega_{\text{coupled}})_o$, can be obtained by differentiating Eq. 45 with respect to ω, which results in

$$(\omega_{\text{coupled}})_o = \frac{2X_e - X_{pe}}{2\,(X_p - X_{pe} + X_e)} \tag{51}$$

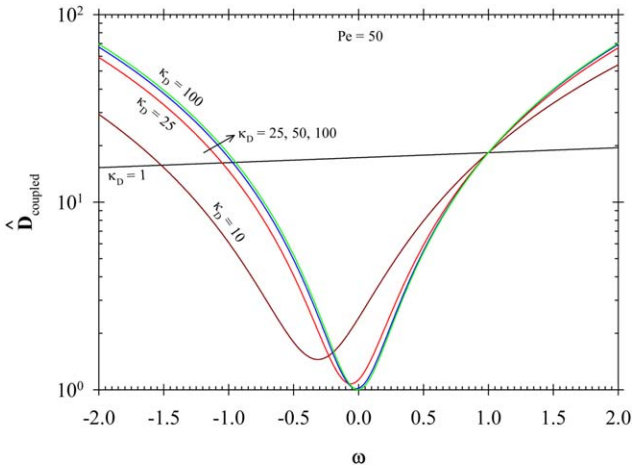

Figure 8. The coupled dispersion coefficients vs. Poiseuille contribution fraction, ω, for different values of the dimensionless Debye–Hückel parameter when $Pe = 50$.

[Color figure can be viewed in the online issue, which is available at wileyonlinelibrary.com.]

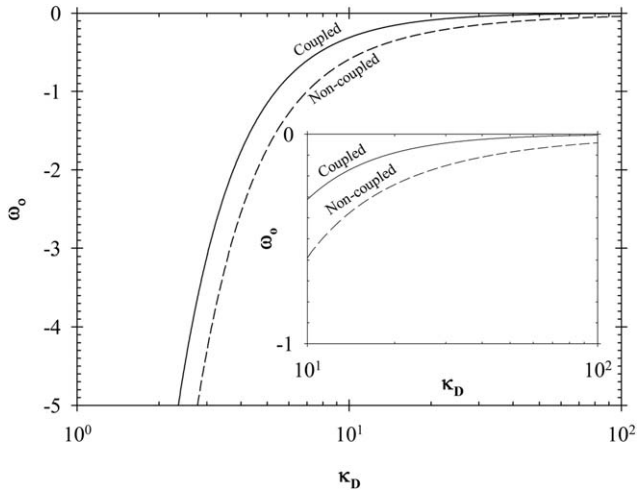

Figure 9. Optimum value of the Poiseuille contribution fraction for the coupled and noncoupled systems vs. κ_D.

Figure 8 also reveals that by decreasing the Debye length the optimum tends to zero for $\kappa_D > 50$, where the coupled dispersion coefficients are almost the same at this condition because the combined flows resemble the same velocity profile for all κ_D values greater than 50. This coupled dispersion coefficient can be obtained by applying Eq. 46 as $\lim \hat{\mathbf{D}}_{\text{coupled}}{}_{\kappa_D \to +\infty} |_{Pe=50} = 1 + (625/36)\,\omega^2$.

By differentiating Eq. 43 with respect to ω, it is possible to obtain an optimum value for the Poiseuille contribution fraction, $(\omega_{\text{noncoupled}})_o$, at which the noncoupled dispersion coefficient, $\hat{\mathbf{D}}_{\text{noncoupled}}$, is minimum

$$(\omega_{\text{noncoupled}})_o = \frac{2Y_{e1} + Y_{e2} - Y_{pe} - Y_{p2}}{2\,(Y_{p1} - Y_{pe} + Y_{e1})} \tag{52}$$

It is interesting to note that $(\omega_{\text{coupled}})_o$ and $(\omega_{\text{noncoupled}})_o$ are functions of κ_D only. Eqs. 51 and 52 are plotted in Figure 9 to provide optimum value of ω_o for the coupled and noncoupled systems vs. κ_D. It is observed that ω_o for the coupled system is larger than that for the noncoupled system. However, $(\omega_{\text{coupled}})_o$ and $(\omega_{\text{noncoupled}})_o$ are always negative (scenario i)

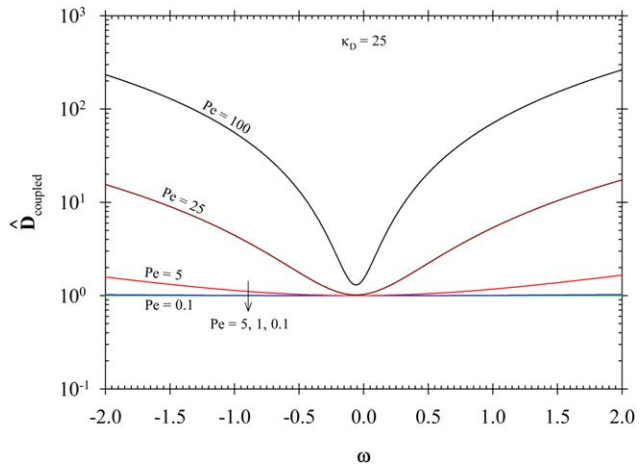

Figure 10. The coupled dispersion coefficients vs. Poiseuille contribution fraction for different values of the Péclet number when κ_D=25.

[Color figure can be viewed in the online issue, which is available at wileyonlinelibrary.com.]

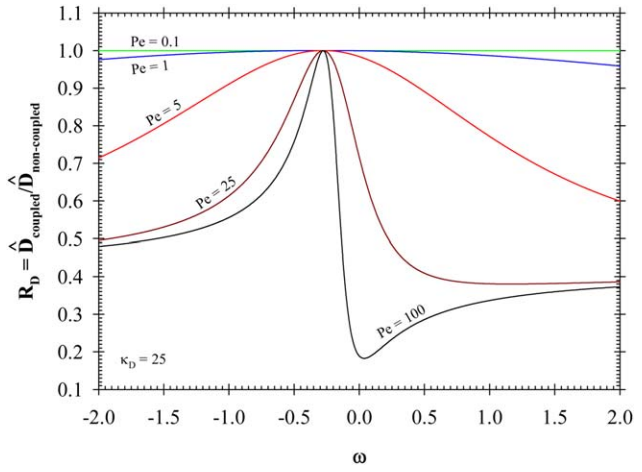

Figure 11. The ratio of the dispersion coefficient in a coupled system to the dispersion coefficient in a noncoupled system vs. Poiseuille contribution fraction for different values of the Péclet number when κ_D=25.

[Color figure can be viewed in the online issue, which is available at wileyonlinelibrary.com.]

and they increase as the dimensionless Debye length increases and approach zero in the limit of a very thin EDL ($\kappa_D \to +\infty$).

The coupled dispersion coefficients described by Eq. 45 are plotted vs. Poiseuille contribution fraction in Figure 10 for several values of the Péclet number and κ_D=25. The results show that $\hat{\mathbf{D}}_{\text{coupled}}$ is almost unity for $Pe < 1$ while it shows a minimum around $\omega = -0.2$ for $Pe > 5$. As it is clear from Figure 10, for $|\omega| > 1$ and $Pe > 5$, $\hat{\mathbf{D}}_{\text{coupled}}$ can be significantly greater than 1.

Figure 11 illustrates the ratio of the dispersion coefficients in the coupled and noncoupled systems vs. Poiseuille contribution fraction for different Pe when κ_D=25 using Eqs. 43 and 45. The ratio is almost unity for low Péclet numbers whereas it increases first and reaches to a maximum value ($R_{\mathbf{D}} = 1$) and then decreases by increasing ω for high Péclet numbers. The results for the latter case reveal that it is required to include the transport of the chemical species from the capillary tube to the porous medium. It is also interesting to note that for all Pe numbers, the coupled dispersion coefficient is less than the noncoupled one. This behavior is expected as the transport of chemical species from the capillary tube and the surrounding porous medium retards the mixing process leading to a lower dispersion coefficient.

Summary and Conclusions

This work presents an analytical model for transport of a neutral nonreacting solute in a coupled system comprised of a capillary tube and a porous medium. The model applies a 2-D advective-diffusive equation with the combined pressure-driven and EOFs in the capillary tube and a 1-D diffusive equation in the porous medium by imposing the continuity of concentrations and mass fluxes along the interface. The effect of mass transfer between the capillary tube and the surrounding porous medium was not considered for derivation of the shear dispersion coefficient in the previous studies and instead a no-flux boundary condition was assumed at the interface between the two media. In this study, we use the Reynolds decomposition technique and a more realistic boundary

condition at the interface to derive the shear dispersion coefficient for solute transport in a capillary tube with sufficiently low wall or zeta potential (<<25 mV) that accounts for the combined effects of pressure-driven and EOFs. The obtained shear dispersion coefficient depends on the dimensionless Debye–Hückel parameter, Poiseuille contribution fraction, and Péclet number.

The developed model is also capable to provide the shear dispersion coefficient for a noncoupled system. The presented noncoupled dispersion coefficient in this study is in agreement with that developed by Datta and Kotamarthi.[1] The ratio of the dispersion coefficient in a coupled system to the one in a noncoupled system reveals that it is essential to include the transport of chemical species from the capillary tube to the surrounding porous medium in development of the dispersion coefficient. The results show that the optimum Poiseuille contribution fraction that minimizes the dispersion of a chemical species inside a capillary tube is always negative. It was also shown that the dispersion can be further reduced in the presence of small countercurrent pressure-driven flow with a Poiseuille contribution fraction slightly below zero.

The obtained results have implications for design of porous microfluidic systems. This model can also find applications in fluid flow through shale and clay rocks, separation of emulsions in microchannel-membrane systems, and electrically assisted transdermal drug delivery. To the best of our knowledge, there are no experimental data relevant to the physical set up studied here in the literature. Therefore, the developed model motivates experimental investigations in this area.

In the analysis presented the influence of solute adsorption on the tube wall was not considered and the tube radius was assumed to be constant. Moreover, further investigations are needed to address some of the assumptions made in this study such as application of the Poisson equation for the electric potential in the EDL, Boltzmann distribution for the charge density in the EDL, adopting the Debye–Hückel linearization for a sufficiently low wall or zeta potential (<<25 mV), and the idea of constant wall or zeta potential for a porous wall.

Acknowledgments

The authors would like to thank the reviewers for their constructive comments. Financial support of NSERC/AI-EES (AERI)/Foundation CMG and AITF (iCORE) Chairs Funds is gratefully acknowledged. The first author is appreciative of the support of his parents, Dariush Dejam and Zahra Fakhari. They have been a source of encouragement and inspiration. Morteza Dejam also would like to thank financial supports and motivations received from the Alberta Innovates - Technology Futures (AITF) Ingenuity Doctoral Scholarship and J.B. Hyne Research Innovation Award in May 2015.

Notation

a = aspect ratio of porous medium thickness to capillary tube radius
C = chemical species concentration
D = effective molecular diffusion coefficient, $m^2\ s^{-1}$
$\mathbf{D}$ = dispersion coefficient, $m^2\ s^{-1}$
$\hat{\mathbf{D}}$ = dimensionless dispersion coefficient
E = electric field, $V\ m^{-1}$
f = coefficient of electro-osmotic velocity
I = modified Bessel function of first kind
L = length of capillary tube, m
p = pressure, Pa
Pe = Péclet number
r = radial coordinate, m
R = radius of capillary tube, m
$R_{\mathbf{D}}$ = ratio of coupled dispersion coefficient to noncoupled dispersion coefficient
t = time, s
u = velocity, $m\ s^{-1}$
x = horizontal coordinate, m
X = factor in coupled dispersion coefficient
Y = factor in noncoupled dispersion coefficient

Greek letters

ϕ = porosity
ω = fraction of combined flow contributed by pressure-driven (Poiseuille) flow
λ = defined function in f
δ = Dirac delta function
β = dimensionless parameter with values of 0 (noncoupled system) and 1 (coupled system)
κ = Debye–Hückel parameter or inverse of Debye length (a measure of EDL thickness), m^{-1}
τ = time scale on order of diffusion time across capillary tube, s
Δp = pressure gradient, Pa
ΔR = thickness of porous medium, m

Subscripts

0, 1 = orders of modified Bessel function of first kind
1, 2 = capillary tube and porous medium
D = dimensionless
$\mathbf{D}$ = dispersion
e = electro-osmotic
in = inlet of capillary tube
o = optimum
out = outlet of capillary tube
p = pressure-driven (Poiseuille)

Superscripts

* = inlet of capillary tube
$-$ = average
$'$ = deviations from average

Literature Cited

1. Datta R, Kotamarthi VR. Electrokinetic dispersion in capillary electrophoresis. *AIChE J*. 1990;36:916–926.
2. Dutta D, Leighton DT. Dispersion in large aspect ratio microchannels for open-channel liquid chromatography. *Anal Chem.* 2003;75:57–70.
3. Zholkovskij EK, Masliyah JH. Hydrodynamic dispersion due to combined pressure-driven and electroosmotic flow through microchannels with a thin double layer. *Anal Chem.* 2004;76:2708–2718.
4. Datta S, Ghosal S. Characterizing dispersion in microfluidic channels. *Lab Chip*. 2009;9:2537–2550.
5. Datta R. Theoretical evaluation of capillary electrophoresis performance. *Biotechnol Prog*. 1990;6:485–493.
6. McEldoon JP, Datta R. Analytical solution for dispersion in capillary liquid chromatography with electroosmotic flow. *Anal Chem.* 1992;64:227–230.
7. Griffiths SK, Nilson RH. Hydrodynamic dispersion of a neutral nonreacting solute in electroosmotic flow. *Anal Chem.* 1999;71:5522–5529.
8. Dutta D, Leighton DT. A low dispersion geometry for microchip separation devices. *Anal Chem.* 2002;74:1007–1016.
9. Zholkovskij EK, Masliyah JH, Czarnecki J. Electroosmotic dispersion in microchannels with a thin double layer. *Anal Chem.* 2003;75:901–909.
10. Ghosal S. Electrokinetic flow and dispersion in capillary electrophoresis. *Annu Rev Fluid Mech.* 2006;38:309–338.
11. Huang HF, Lai CL. Enhancement of mass transport and separation of species by oscillatory electroosmotic flows. *Proc R Soc A*. 2006;462:2017–2038.
12. Ramon G, Agnon Y, Dosoretz C. Solute dispersion in oscillating electro-osmotic flow with boundary mass exchange. *Microfluid Nanofluid.* 2011;10:97–106.
13. Paul S, Ng CO. Dispersion in electroosmotic flow generated by oscillatory electric field interacting with oscillatory wall potentials. *Microfluid Nanofluid.* 2012;12:237–256.

14. Paul S, Ng CO. On the time development of dispersion in electroosmotic flow through a rectangular channel. *Acta Mech Sin*. 2012;28:631–643.
15. Ng CO, Zhou Q. Dispersion due to electroosmotic flow in a circular microchannel with slowly varying wall potential and hydrodynamic slippage. *Phys Fluids*. 2012;24:112002.
16. Song J, Ng CO, Law WKA. Dispersion in oscillatory electro-osmotic flow through a parallel-plate channel with kinetic sorptive exchange at walls. *J Hydrodynam B*. 2014;26:363–373.
17. Taylor G. Dispersion of soluble matter in solvent flowing slowly through a tube. *Proc R Soc London A*. 1953;219:186–203.
18. Taylor JA, Yeung ES. Imaging of hydrodynamic and electrokinetic flow profiles in capillaries. *Anal Chem*. 1993;65:2928–2932.
19. Herr AE, Molho JI, Santiago JG, Mungal MG, Kenny TW, Garguilo MG. Electroosmotic capillary flow with nonuniform zeta potential. *Anal Chem*. 2000;72:1053–1057.
20. Tallarek U, Rapp E, Scheenen T, Bayer E, Van As H. Electroosmotic and pressure-driven flow in open and packed capillaries: velocity distributions and fluid dispersion. *Anal Chem*. 2000;72:2292–2301.
21. Scales N, Tait RN. Modeling electroosmotic and pressure-driven flows in porous microfluidic devices: zeta potential and porosity changes near the channel walls. *J Chem Phys*. 2006;125:094714.
22. Gas B, Stedry M, Kenndler E. Peak broadening in capillary zone electrophoresis. *Electrophoresis*. 1997;18:2123–2133.
23. Berkowitz B, Zhou J. Reactive solute transport in a single fracture. *Water Resour Res*. 1996;32:901–9013.
24. Wang L, Cardenas MB, Deng W, Bennett PC. Theory for dynamic longitudinal dispersion in fractures and rivers with Poiseuille flow. *Geophys Res Lett*. 2012;39:L05401.
25. Smith R. Effect of boundary absorption upon longitudinal dispersion in shear flows. *J Fluid Mech*. 1983;134:161–177.
26. Beard DA, Wu F. Apparent diffusivity and Taylor dispersion of water and solutes in capillary beds. *Bull Math Biol*. 2009;71:1366–1377.
27. Shaw S, Ganguly S, Sibanda P, Chakraborty S. Dispersion characteristics of blood during nanoparticle assisted drug delivery process through a permeable microvessel. *Microvasc Res*. 2014;92:25–33.
28. Griffiths IM, Howell PD, Shipley RJ. Control and optimization of solute transport in a thin porous tube. *Phys Fluids*. 2013;25:033101.
29. Roubinet D, Dreuzy JR, Tartakovsky DM. Semi-analytical solutions for solute transport and exchange in fractured porous media. *Water Resour Res*. 2012;48:W01542.
30. Heße F, Prykhodko V, Attinger S. Assessing the validity of a lower-dimensional representation of fractures for numerical and analytical investigations. *Adv Water Resour*. 2013;56:35–48.
31. Dejam M, Hassanzadeh H, Chen Z. Shear dispersion in a fracture with porous walls. *Adv Water Resour*. 2014;74:14–25.
32. Dejam M, Hassanzadeh H, Chen Z. Shear dispersion in a capillary tube with a porous wall. *J. Contam Hydrol*. Revision submitted for publication.
33. Ghosal S. The effect of wall interactions in capillary-zone electrophoresis. *J Fluid Mech*. 2003;491:285–300.
34. Datta S, Ghosal S. Dispersion due to wall interactions in microfluidic separation systems. *Phys Fluids*. 2008;20:012103.
35. Vennela N, Bhattacharjee S, De S. Sherwood number in porous microtube due to combined pressure and electroosmotically driven flow. *Chem Eng Sci*. 2011;66(24):6515–6524.
36. Vennela N, Mondal S, De S, Bhattacharjee S. Sherwood number in flow through parallel porous plates (Microchannel) due to pressure and electroosmotic flow. *AIChE J*. 2012;58(6):1693–1703.
37. Revil A, Pessel M. Electroosmotic flow and the validity of the classical Darcy equation in silty shales. *Geophys Res Lett*. 2002;29:14-1–14-4.
38. Revil A, Leroy P. Constitutive equations for ionic transport in porous shales. *J Geophys Res*. 2004;109:B03208.
39. Jougnot D, Revil A, Lu N, Wayllace A. Transport properties of the Callovo-Oxfordian clay rock under partially saturated conditions. *Water Resour Res*. 2010;46:W08514.
40. Revil A, Woodruff WF, Lu N. Constitutive equations for coupled flows in clay materials. *Water Resour Res*. 2011;47:W05548.
41. Paineau E, Bihannic I, Baravian C, Philippe AM, Davidson P, Levitz P, Funari SS, Rochas C, Michot LJ. Aqueous suspensions of natural swelling clay minerals. *1. Structure and electrostatic interactions. Langmuir*. 2011;27:5562–5573.
42. Watson JD, Baker TA, Bell SP, Gann A, Levine M, Losick R. *Molecular Biology of the Gene*. New York: Cold Spring Harbor Lab Press, 2004.
43. Wightman RM. Probing cellular chemistry in biological systems with microelectrodes. *Science*. 2006;311:1570–1574.
44. Vafai K. *Porous Media: Applications in Biological Systems and Biotechnology*. New York: CRC Press, Taylor & Francis Group, 2011.
45. Burnette R, Marrero D. Comparison between the iontophoretic and passive transport of thyrotropin releasing hormone across excised nude mouse skin. *J Pharm Sci*. 1986;75:738–743.
46. Siddiqui O, Sun Y, Liu JC, Chien YW. Facilitated transdermal transport of insulin. *J Pharm Sci*. 1987;76:341–345.
47. Liu C, Sun Y, Siddiqui O, Chien YW, Shi WM, Li J. Blood glucose control in diabetric rats by transdermal iontophoretic delivery of insulin. *Int J Pharm*. 1988;44:197–204.
48. Kim A, Green PG, Rao G, Guy RH. Convective solvent flow across the skin during iontophoresis. *Pharm Res*. 1993;10:1315–1320.
49. Zhang I, Shung KK, Edwards DA. Hydrogels with enhanced mass transfer for transdermal drug delivery. *J Pharm Sci*. 1996;85:1312–1316.
50. Riviere JE, Heit MC. Electrically-assisted transdermal drug delivery. *Pharm Res*. 1996;14:687–697.
51. Banga AK, Chien YW. Iontophoretic delivery of drugs: fundamentals, developments, and biomedical applications. *J Control Release*. 1998;7:1–24.
52. Guy RH, Kalia YN, Delgado-Charro MB, Merino V, López A, Marro D. Iontophoresis: electrorepulsion and electroosmosis. *J Control Release*. 2000;64:129–132.
53. Sieg A, Guy RH, Delgado-Charro MB. Electroosmosis in transdermal iontophoresis: implications for noninvasive and calibration-free glucose monitoring. *Biophys J*. 2004;87:3344–3350.
54. Brown MB, Trayanor MJ, Martin GP, Franklin AK. Transdermal drug delivery systems. In: Jain KK, Editor. *Drug Delivery Systems*. New Jersey: Humana Press, 2008:119–124.
55. Khan A, Yasir M, Asif M, Chauhan I, Singh AP, Sharma R, Singh P, Rai S. Iontophoretic drug delivery: history and applications. *J Appl Pharm Sci*. 2011;1(3):11–24.
56. Molla SH, Bhattacharjee S. Prevention of colloidal membrane fouling employing dielectrophoretic forces on a parallel electrode array. *J Memb Sci*. 2005;255:187–199.
57. Molla SH, Masliyah JH, Bhattacharjee S. Simulation of dielectrophoretic membrane filtration process for removal of water droplets from water-in-oil emulsions. *J Colloid Inetrface Sci*. 2005;287:338–350.
58. Xu Y. Tutorial: capillary electrophoresis. *Chem Educ*. 1996;1(2):1–14.
59. Bird RB, Stewart WE, Lightfoot EN. *Transport Phenomena*. New York: Wiley, 1960.
60. Deen W. *Analysis of Transport Phenomena: Topics in Chemical Engineering*. New York: Oxford University Press, 1998.
61. Probstein RF. *Physicochemical Hydrodynamics: An Introduction*. New York: Wiley, 2005.
62. Fischer HB, List EJ, Koh RCY, Imberger J, Brooks NH. *Mixing in Inland and Coastal Waters*. San Diego: Academic, 1979.
63. Bear J. *Dynamics of Fluids in Porous Media*. New York: American Elsevier Publishing Company, Inc., 1972.
64. Cussler EL. *Diffusion: Mass Transfer in Fluid Systems*. New York: Cambridge University Press, 2007.
65. Bowman F. *Introduction to Bessel Functions*. New York: Dover, 1958.
66. Kuo CY, Wang CY, Chang CC. Generation of directional EOF by interactive oscillatory zeta potential. *Electrophoresis*. 2008;29:4386–4390.
67. Al-Hadhrami AK, Elliott L, Ingham DB, Wen X. Analytical solutions of fluid flows through composite channels. *J Porous Media*. 2001;4:149–163.

Appendix A: The Lommel[65] and other Integrals Accompanied with the Modified Bessel Functions of the First Kind of Order 2 and 3 (I_2, I_3)

The Lommel[65] integral, which involves the modified Bessel functions of the first kind of order 0 and 1 (I_0, I_1), is defined as follows[65]

$$\int r_D I_0^2(\kappa_D r_D)\, dr_D = \frac{1}{2} r_D^2 [I_0^2(\kappa_D r_D) - I_1^2(\kappa_D r_D)] \tag{A1}$$

The other integrals involving the modified Bessel functions of the first kind of order 0 and 1 (I_0, I_1) are presented as below[65]

$$\int I_1(\kappa_D r_D)\, dr_D = \frac{1}{\kappa_D} I_0(\kappa_D r_D) \tag{A2}$$

$$\int r_D I_0(\kappa_D r_D)\, dr_D = \frac{1}{\kappa_D} r_D I_1(\kappa_D r_D) \tag{A3}$$

$$\int r_D^3 I_0(\kappa_D r_D)\, dr_D = \frac{1}{\kappa_D^2} r_D^2 [2I_2(\kappa_D r_D) + \kappa_D r_D I_3(\kappa_D r_D)] \tag{A4}$$

$$\int r_D^5 I_0(\kappa_D r_D)\, dr_D = \frac{1}{\kappa_D^3} r_D^3 (\kappa_D^2 r_D^2 + 8) I_3(\kappa_D r_D) \tag{A5}$$

The modified Bessel functions of the first kind of order 2 and 3 (I_2, I_3) as functions of the modified Bessel functions of the first kind of order 0 and 1 (I_0, I_1) are as follows[65]

$$I_2(\kappa_D r_D) = I_0(\kappa_D r_D) - \frac{2}{\kappa_D r_D} I_1(\kappa_D r_D) \tag{A6}$$

$$I_3(\kappa_D r_D) = -\frac{4}{\kappa_D r_D} I_0(\kappa_D r_D) + \left[1 + \frac{8}{(\kappa_D r_D)^2}\right] I_1(\kappa_D r_D) \tag{A7}$$

Equations A4 and A5 can be expressed as functions of the modified Bessel functions of the first kind of order 0 and 1 (I_0, I_1) using Eqs. A6 and A7

$$\int r_D^3 I_0(\kappa_D r_D)\, dr_D = \frac{1}{\kappa_D^2} r_D^2 \left[-2I_0(\kappa_D r_D) + \left(\kappa_D r_D + \frac{4}{\kappa_D r_D}\right) I_1(\kappa_D r_D)\right] \tag{A6}$$

$$\int r_D^5 I_0(\kappa_D r_D)\, dr_D = \frac{1}{\kappa_D^3} r_D^3 (\kappa_D^2 r_D^2 + 8) \left[-\frac{4}{\kappa_D r_D} I_0(\kappa_D r_D) + \left(1 + \frac{8}{(\kappa_D r_D)^2}\right) I_1(\kappa_D r_D)\right] \tag{A7}$$

Appendix B: Implementation of the Ratio of the Modified Bessel Functions of the First Kind of Order 0 and 1, $I_1(\kappa_D)/I_0(\kappa_D)$

Due to the exponential nature of the modified Bessel functions of the first kind of order 0 and 1 [$I_0(\kappa_D)$, $I_1(\kappa_D)$], the MATLAB implementation of these functions could only be computed for $\kappa_D \leq 709.7$. However, the functional form of these equations can be rewritten in such a way that enables computation for $\kappa_D > 709.7$.[21,67] The asymptotic form for the modified Bessel function of the first kind of order 0, $I_0(\kappa_D)$, when $\kappa_D \to +\infty$ is[65]

$$I_0(\kappa_D) \approx \sqrt{\frac{1}{2\pi\kappa_D}} e^{\kappa_D} \tag{B1}$$

Noting that $dI_0(\kappa_D)/d\kappa_D = I_1(\kappa_D)$, the asymptotic form for the modified Bessel function of the first kind of order 1, $I_1(\kappa_D)$, is[65]

$$I_1(\kappa_D) \approx \sqrt{\frac{1}{2\pi\kappa_D}} e^{\kappa_D} \left(1 - \frac{1}{2\kappa_D}\right) \tag{B2}$$

Therefore, the ratio of the modified Bessel functions of the first kind of order 0 and 1, $I_1(\kappa_D)/I_0(\kappa_D)$, can be calculated as follows using Eqs. B1 and B2

$$\frac{I_1(\kappa_D)}{I_0(\kappa_D)} \approx 1 - \frac{1}{2\kappa_D} \tag{B3}$$

These relations extend the range of computation of the above functions for $\kappa_D > 709.7$.

Manuscript received Nov. 6, 2014, and revision received May 2, 2015.